ADVANCED FUNCTIONAL MATERIALS

FULL PAPER

Three-Dimensional Porous Copper–Tin Alloy Electrodes for Rechargeable Lithium Batteries**

By *Heon-Cheol Shin* and *Meilin Liu**

Three-dimensional (3D) foam structure of a Cu_6Sn_5 alloy was fabricated via an electrochemical deposition process. The walls of the foam structure are highly porous and consist of numerous small grains. When used as a negative electrode for a rechargeable lithium battery, the Cu_6Sn_5 samples delivered a reversible capacity of about 400 mA h g^{-1} up to 30 cycles. Further, these materials exhibit superior rate capability, attributed primarily to the unique porous structure and the large surface area for fast mass transport and rapid surface reactions. For instance, at a current drain of 10 mA cm^{-2} (20C rate), the obtainable capacity (220 mA h g^{-1}) was more than 50 % of the capacity at 0.5 mA cm^{-2} (1C rate).

1. Introduction

The demand for electrode materials with higher reversible capacity than carbon-based materials has stimulated researchers to explore many different types of materials as the negative electrode for lithium batteries.[1–3] Among them, tin has been widely studied because of its much higher theoretical capacity (991 mA h g^{-1}; 7200 mA h cc^{-1}) than graphite (372 mA h g^{-1}; 837 mA h cc^{-1}).[4–6] However, the poor cyclability due to large volume change (up to 360 %) during cycling makes it impractical to use pure tin metal as electrode for rechargeable lithium batteries,[4] despite the fact that many attempts have been made to improve the cycling stability. Recently, tin-based intermetallic compounds Sn_xMe_y (Me: inactive element) have been reported as promising electrode materials, including Cu–Sn,[7–10] Ni–Sn,[11–13] and Fe–Sn[14,15] systems. The reaction of the intermetallic compounds Sn_xMe_y with lithium has been described as the formation of brittle Li–Sn alloys within a relatively soft (ductile) inactive matrix Me, which buffers the large volume change in the course of alloying processes.[16,17] Accordingly, the Sn_xMe_y can provide a much more stable cycling performance than pure tin metal and at the same time still offer larger reversible specific (gravimetric and/or volumetric) capacity as compared to graphite.

In a recent communication,[18] three-dimensional (3D) metal foam structures (of copper and tin) with nano-dendritic walls have been fabricated using an electrochemical deposition process. This unique porous structure is attributed to the concurrent generation of hydrogen bubbles with extremely fast metal deposition at high cathodic current densities. The porous foam structure would allow not only fast transport of lithium ions through the electrolyte and the electrode (due to short diffusion length) but also rapid electrochemical reactions (due to high surface area), resulting in a high-performance anode for lithium batteries with superior rate capability. Here, we report the detailed microscopic features and the electrochemical performance of a highly open, porous Cu–Sn intermetallic compound, η'-Cu_6Sn_5, prepared via an electrochemical deposition process.

2. Results and Discussion

Shown in Figure 1 are some typical scanning electron microscopy (SEM) images of porous copper–tin alloys, created by an electrochemical deposition process for different periods of time. The deposited films were characterized by a 3D foam structure. The origin of this unique structure is as discussed elsewhere[18] and briefly summarized as follows. Since the hydrogen over-voltage of the copper substrate is low to generate hydrogen gas in highly acidic media and at high cathodic current densities,[19] a large number of hydrogen bubbles created on the copper substrate move towards the electrolyte/air interface during the electrodeposition process. Thus, the metal growth towards the gas bubble is prohibited simply because there are no metal ions available there, leading to deposition only between gas bubbles. In other words, the hydrogen bubbles function as a dynamic template during metal deposition when deposition parameters are carefully selected, includ-

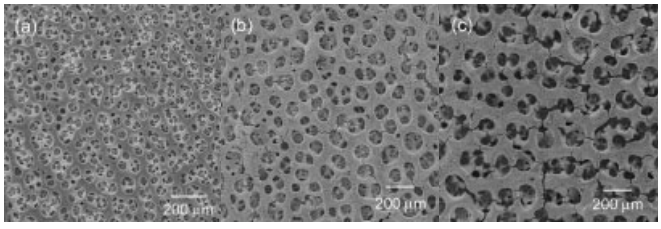

Figure 1. Typical SEM images of porous Cu–Sn alloys created by an electrochemical deposition process for different periods of time: a) 5 s, b) 10 s, and c) 20 s.

[*] Prof. M. Liu, Dr. H.-C. Shin
Center for Innovative Fuel Cell and Battery Technologies
School of Materials Science and Engineering,
Georgia Institute of Technology
Atlanta, GA 30332-0245 (USA)
E-mail: meilin.liu@mse.gatech.edu

[**] This work was supported by the Office of Science, Department of Energy under Grant No. DE-FG02-01ER15220.

  DOI: 10.1002/adfm.200305165

ADVANCED FUNCTIONAL MATERIALS

ing the concentrations of Cu/Sn sulfates and sulfuric acid as well as the applied current densities. The effect of deposition parameters on the morphology of the foam structure can be found elsewhere.[18]

As depicted in Figure 1, the surface pore size of the foam increases with the time of deposition, which is attributed to the coalescence of hydrogen bubbles generated during electrodeposition. It is noted that the pore walls are partially cracked and the crack formation becomes severe as the deposition time (i.e., film thickness) increases. The partial cracking of the deposits is probably a consequence of the stresses induced by vigorous hydrogen evolution under extreme deposition conditions, damaging the continuous structure of the foam walls.

Figure 2 shows the typical microstructures of a copper–tin deposit at different magnifications. Clearly, the walls of the foam are highly porous and contain numerous small grains. It is conceivable that the large pores of the foam structure, seen in Figure 2a, are created by the hydrogen bubbles evolved from the copper substrate, whereas the small pores inside the walls, seen in Figure 2c, originate mainly from the hydrogen bubbles liberated from the freshly formed porous deposits of copper–tin alloys.[20] Although the large nodules (of the size of about 1 μm) resulting from the aggregation of small particles are sporadically observed through the foam walls, the feature size of the particles in the foam walls is of the order of hundreds of nanometers (Fig. 2c). While the average size of the large pores of the foam structure increased with the deposition time, the size of the small pores and the microstructures of the foam wall remain similar, implying that the well-defined microstructures are uniformly created throughout the foam structure.

The powders of the deposits (scratched from the substrates) typically have surface area of about 20 $m^2 g^{-1}$, as measured using the Brunauer–Emmett–Teller (BET) technique (ASAP 2000, Micromeritics). Based on the BET results, the equivalent particle size of the Cu_6Sn_5 alloys was estimated to be about 363 nm, assuming that the particles are spherical and that there is no contact among the particles. The calculated particle size matches satisfactorily the observed particle size from SEM, implying that the effect of other factors is relatively small, including the roughness of the particle, interconnection between the particles, and the increase in surface area due to the scratching of the coatings off the substrates. From the rough calculation from the BET result, the surface area of the electrode deposited for 5 s is about 160 times that of a dense electrode film of the same superficial area.

Shown in Figure 3 is an X-ray diffraction (XRD) pattern of the copper–tin alloy scratched from the substrate. The XRD pattern is in good agreement with those reported for low-temperature modification of Cu_6Sn_5, i.e., η'-Cu_6Sn_5, which is known to have a monoclinic lattice with a space-group symmetry of $C2/c$.[21,22] The elemental analysis of the deposits using energy-dispersive X-ray spectroscopy (EDS) showed that the atomic ratio of Cu to Sn is 1.18, which matches the expected atomic ratio of Cu to Sn in η'-Cu_6Sn_5.

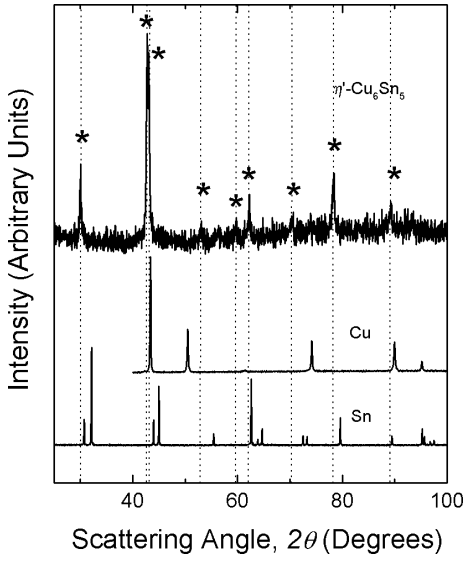

Figure 3. XRD patterns of the powders of Cu–Sn alloy (upper) scratched from the substrate showing that the electrodeposit is an intermetallic compound η'-Cu_6Sn_5 with high crystallinity. The XRD patterns of electrodeposited Cu and Sn (lower) are also given for the sake of comparison [18]. Further details of the crystal-structure investigation(s) may be obtained from the Fachinformationszentrum Karlsruhe, D-76344 Eggenstein-Leopoldshafen (Germany), on quoting the depository numbers CSD-413 067 (Cu), 413 068 (Sn), and 413 560 (Cu_6Sn_5).

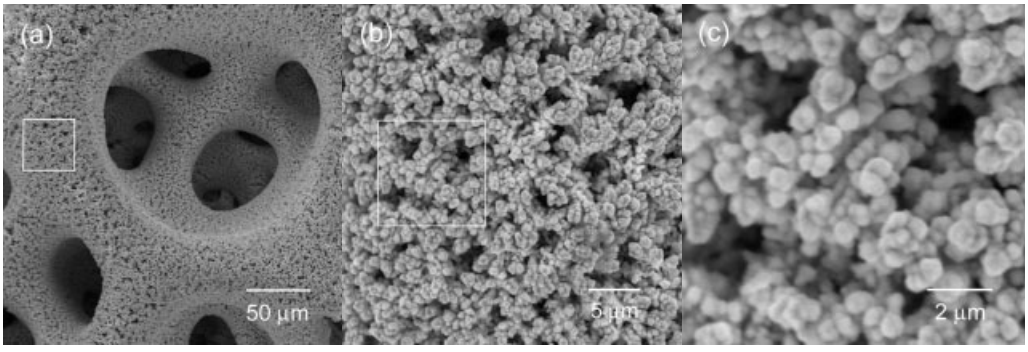

Figure 2. 3D foam structure of a porous Cu–Sn alloy sample (created for 10 s) at different magnification showing that a) the large pores formed due to evolution of H_2 from the substrate, b) the detailed microstructure of the walls, and c) the small pores within the walls formed by the evolution of H_2 from the deposited Cu–Sn particles.

Figure 4a shows the typical voltage versus specific capacity of a Cu_6Sn_5 sample (created for 10 s) for the five cycles (16th–20th) at a current density of 0.5 mA cm^{-2} (1C rate), implying that Cu_6Sn_5 reacted reversibly with lithium to deliver a reversible capacity of about 400 mA h g^{-1}. The differential capacity curve dC/dE shown in Figure 4b, which is reconstructed from the voltage profile for the 16th cycle, showed two distinct reduction peaks, R_1 (at 0.30 V) and R_2 (at <0.01 V), and the two corresponding oxidation peaks, O_1 (at 0.5–0.7 V) and O_2 (at 0.83 V), of Cu_6Sn_5.[8,23]

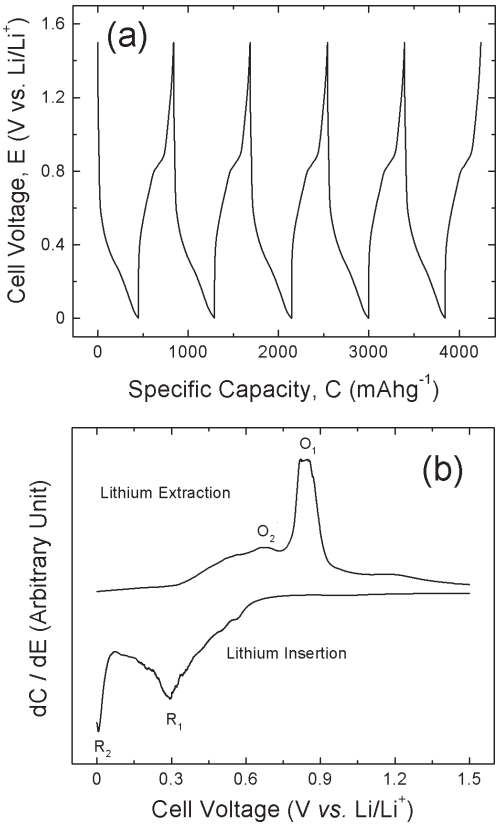

Figure 4. a) Typical voltage profiles of the Cu_6Sn_5 sample (created for 10 s) for the five cycles (16th–20th cycle) at a current density of 0.5 mA cm^{-2} (1C rate) and b) the differential capacity curve, reconstructed from the voltage profile for the 16th cycle.

Although the exact reaction mechanism of Cu_6Sn_5 with lithium is still not clearly understood, especially the formation of the several intermediate ternary phases of Li–Cu–Sn during the lithium alloying/dealloying process,[23,24] it is generally accepted that the reduction peak of R_1 is attributed to the formation of Li_2CuSn, resulting from the alloying of Cu_6Sn_5 with lithium, while the reduction peak R_2 corresponds to the formation of the fully lithiated Sn phase (i.e., $Li_{4.4}Sn$). The corresponding reverse reactions, i.e., the formations of Li_2CuSn and Cu_6Sn_5 are responsible for the oxidation peaks of O_2 and O_1, respectively.

$$10\mathrm{Li} + \mathrm{Cu_6Sn_5} \underset{O_1}{\overset{R_1}{\rightleftarrows}} 5\mathrm{Li_2CuSn} + \mathrm{Cu} \quad (1)$$

$$12Li + 5\mathrm{Li_2CuSn} \underset{O_2}{\overset{R_2}{\rightleftarrows}} 5\mathrm{Li_{4.4}Sn} + 5\mathrm{Cu} \quad (2)$$

Shown in Figure 5 are the variations of the specific capacity with the number of cycles. The plot is roughly divided into three regions. The capacity increases during the first ten cycles (the 1st region), then remains relatively constant between the 10th and the 30th cycle (the 2nd region), and finally decreases rapidly after the 30th cycle (the 3rd region), irrespective of the lithium insertion (solid square) and extraction (solid circle).

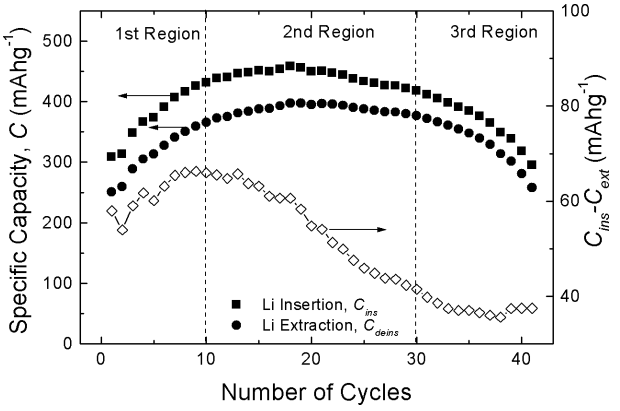

Figure 5. Variation of the specific capacity (solid symbols) and the irreversible capacity loss (open diamonds) of the Cu_6Sn_5 sample (created for 10 s) with the number of cycles at a current density of 0.5 mA cm^{-2} (1C rate).

It is noticeable that the amount of cathodic charge for lithium insertion is always larger than the amount of anodic charge for lithium extraction, implying that the electrode exhibits some irreversible capacity at each cycle. The irreversible capacity loss might be attributed to 1) the inability for all extruded copper to be re-incorporated into the tin flame,[24] 2) mechanical disintegration caused by severe volume change during cycling (e.g., about 45 % volume change during phase transition from Cu_6Sn_5 to Li_2CuSn), 3) formation of lithium oxides (Li_2O) from the Cu_xO and SnO_x impurities which can be formed during the electrochemical deposition in an aqueous bath, and 4) formation of a solid electrolyte interphase (SEI) layer on the surface. The latter two are expected to be more pronounced in our nanostructured alloy electrodes because of the nanostructure and large surface/interface areas.

Interestingly, the amount of the irreversible capacity, C_{ins}–C_{ext} (◇ in Fig. 5), initially increased with cycling (see in the 1st region), implying that new source for irreversible capacity loss may become active. Considering that the foam-wall thickness of the electrodeposited Cu_6Sn_5 alloy is of the order of tens of micrometers as shown in Figure 2a, it is conceivable that some of the active material was isolated during cell fabrication. The isolated material may become active as the electrolyte penetrates into the porous structure with cycling because of the dramatic volumetric and morphological change.

Assuming the isolated active materials inside the walls are exposed to the electrolyte at each cycle throughout the cycling

ADVANCED FUNCTIONAL MATERIALS

test, the variation of capacity retention and irreversible capacity with number of cycle can be explained as follows. In the first region, a large amount of Cu_6Sn_5 active materials are freshly exposed to the electrolyte and the increase in capacity by this newly exposed alloys overwhelms the decrease in capacity due to the above reasons (1) and (2), increasing the total specific capacity. While the creation of new active volume increases the capacity, it is detrimental to the charge/discharge efficiency due to the reasons (1) to (4). In the second region, the generation of new active volume is significantly suppressed and is balanced with the degradation of the electrode, making the capacity retention almost constant. The decrease in the newly created active volume leads to the increase in the efficiency since the reactions of (3) and (4) are suppressed. Finally, in the third region, the amount of newly created active volume is quite small and hence the total capacity is considerably reduced.

Shown in Figure 6 is the rate capability of a Cu_6Sn_5 sample (deposition time: 10 s). Before the rate-capability test, the electrodeposited samples were activated initially by cycling about ten times at 1C rate so that the capacity retention remained the same during the subsequent rate-capability test. In other words, the rate-capability experiment was performed in the 2nd region of Figure 5.

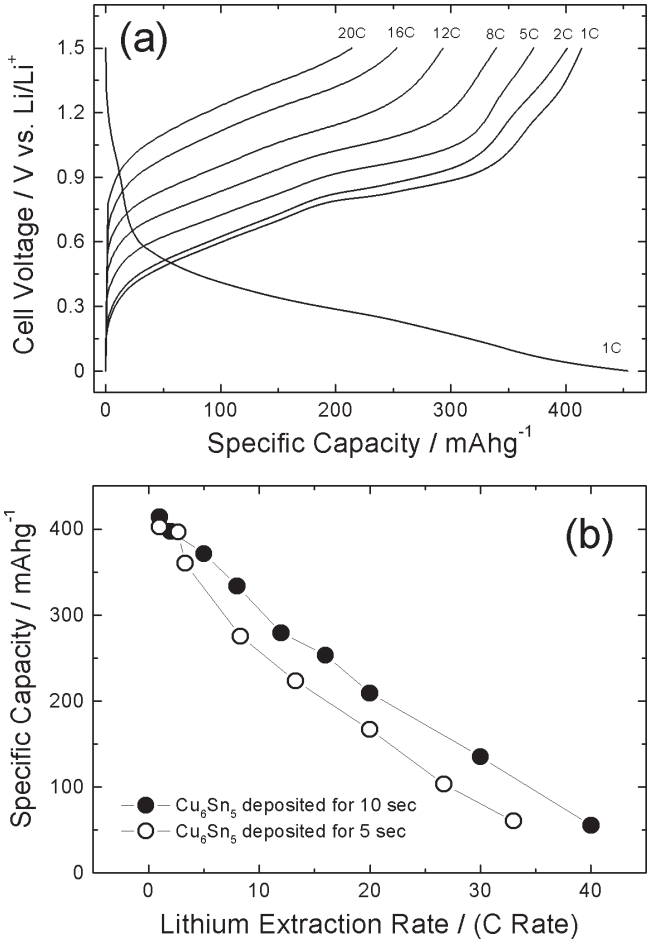

Figure 6. a) Dependence of the voltage profile on applied current densities for the Cu_6Sn_5 sample created for 10 s and b) variation of specific-capacity retentions of the Cu_6Sn_5 samples created for 10 s (●) and 5 s (○) with lithium-extraction rate.

At the lithium-extraction rates of 1C (0.5 mA cm^{-2}), 2C (1.0), 5C (2.5), 8C (4), 12C (6), 16C (8), and 20C (10), the Cu_6Sn_5 deposit delivered the specific capacities of 420 mA h g^{-1}, 400, 380, 345, 300, 255, and 220, respectively. Figure 6b summarizes the rate capability in a chronological order. Each point in Figure 6b was determined by averaging the values during three repetitive cycles under the same current drain. The capacity retention decreased gradually with increasing lithium extraction rate. In particular, about 50 % of the reversible capacity at 1C rate can be delivered at an extremely high rate, 20C (i.e., within 3 min.). To the best of our knowledge, this represents the highest rate capability of an Sn or Sn-based alloy ever reported.[9,25]

The rate capability of the Cu_6Sn_5 alloy prepared in 5 s (○ in Fig. 6b) showed similar trend to that of the sample prepared in 10 s. Nevertheless, the rate capability of 10 s deposited sample is slightly better than that of 5 s deposited sample at high lithium-extraction rates (> 3C rate). This result indicates that there are subtle differences in the foam structure between two samples, yielding a slightly different ability to meet high current density. However, we could not find a noticeable difference in the wall structure between two samples on their micrographs, implying the difference in rate performance could originate from the whole 3D architecture, not just microstructures. Under the circumstances, we suggest that the large pores (on average) of the 10 s deposited sample could be more favorable to fast lithium-ion transport at high current density than the small pores of the 5 s deposited sample. For example, the lithium-extraction process at a 20C rate would be complete in 3 min. Within this short time, it is expected that 10 s deposited foam with large pore sizes (220 mA h g^{-1}) can allow a larger amount of lithium ions to be transported from the porous structure to the bulk electrolyte as a result of lower mass-transport polarization through the foam structure, than 5 s deposited foam with small pore sizes (166 mA h g^{-1}). After a series of rate-capability tests, the capacity retention of the Cu_6Sn_5 sample at 1C was still about 85 %, implying that capacity fade during the rate-capability tests was about 15 %.

On the other hand, the capacity retention of the Cu_6Sn_5 alloy deposited for 20 s was below 10 % after five galvanostatic cycles, making further electrochemical characterizations (including rate-performance test) meaningless. One possible reason for this rapid capacity fade is the poor contact between active materials and substrate. The energetic hydrogen evolution during an alloy-deposition process could make the active materials loosely adhered to the substrate and thus the active materials are readily disintegrated from the substrate in the course of lithium alloying/dealloying process. Similarly, the contact problem can be partly responsible for the poor cycling stability of the 10 s deposited sample (Fig. 5). In order to strengthen the contact between active material and substrate, a couple of methods are being tested, including the control of the amount/size of the evolved hydrogen bubble and post-annealing of the deposits.

3. Conclusions

Three-dimensional foam structure of a Cu_6Sn_5 alloy was successfully created using an electrochemical deposition process. The foam structure is characterized by highly porous foam walls consisting of active small grains of Cu_6Sn_5 alloy. The electrochemical measurements showed that the porous Cu_6Sn_5 samples delivered a reversible capacity of about 400 mA h g^{-1} up to 30 cycles as a negative electrode for lithium batteries. Furthermore, at an extremely high current drain of 20C rate, the capacity retention was about 50 % of the capacity at 1C rate. Although the cycling stability needs to be improved for practical applications, the excellent rate capability of the present Cu_6Sn_5 sample opens up new possibility for constructing unique 3D nanostructured electrodes for rechargeable lithium batteries.

4. Experimental

Preparation and Characterization of the 3D Porous Copper–Tin Alloy: High-purity copper (Alfa Aesar, 99.8 %), cleaned with acetone and dilute hydrochloric acid, was used as the substrate (cathode) for copper–tin alloy deposition. A Platinum wire was used as the counter electrode (anode). The distance between anode and cathode was kept at 2 cm. For copper–tin alloy deposition, a constant current (as high as 5 A cm^{-2}) was applied to the cell using a Solartron 1285 potentiostat in an electrolyte of 1.5 M sulfuric acid (Aldrich) containing 0.24 M copper sulfate and 0.20 M tin sulfate. Deposition was performed at room temperature in a stationary electrolyte solution (with neither stirring nor N_2 bubbling). The electrode loading on the copper substrate was proportional to the deposition time with a proportionality constant of 0.16 mg cm^{-2} s^{-1}. The morphologies of the deposited films were revealed using a scanning electron microscope (Hitachi S-800 Field-Emission SEM). For structural characterization, the deposits were scratched from the substrate and the powder X-ray diffraction (XRD) pattern was recorded using a Philips PW-1800 X-Ray Diffractometer (with Cu Kα radiation).

Electrochemical Testing: A three-electrode electrochemical cell was employed for all electrochemical measurements using lithium foils as the counter and reference electrodes. A 1 M solution of $LiPF_6$ in a 50:50 (v/v) mixture of ethylene carbonate (EC) and diethyl carbonate (DEC) was used as the electrolyte. All cells were assembled and tested in a glove-box (Vacuum Atmospheres Company, U.S.A.) filled with purified Ar gas. A Solartron 1285 potentiostat was employed to carry out constant-current cell cycling. In particular, for the rate-capability test, cathodic currents of 0.25 and 0.5 mA cm^{-2} (1C rate [26]) were applied to the active materials deposited for 5 s and 10 s, respectively, until the cell voltage reached 0.0 V (versus Li/Li^+). Subsequently, anodic currents ranging from 1C to 40C rate were applied until the cell voltage reached 1.5 V (versus Li/Li^+).

Received: December 4, 2003
Final version: August 6, 2004

[1] M. Winter, J. O. Besenhard, M. E. Spahr, P. Novak, *Adv. Mater.* **1998**, *10*, 725.
[2] J. M. Tarascon, M. Armand, *Nature* **2001**, *414*, 359.
[3] R. A. Huggins, *Solid State Ionics* **2002**, *152–153*, 61.
[4] I. A. Courtney, J. R. Dahn, *J. Electrochem. Soc.* **1997**, *144*, 2045.
[5] M. Winter, J. O. Besenhard, *Electrochim. Acta* **1999**, *45*, 31.
[6] R. A. Huggins, *J. Power Sources* **1999**, *81/82*, 13.
[7] K. D. Kepler, J. T. Vaughey, M. M. Thackeray, *Electrochem. Solid-State Lett.* **1999**, *2*, 307.
[8] G. X. Wang, L. Sun, D. H. Bradhurst, S. X. Dou, H. K. Liu, *J. Alloys Compd.* **2000**, *299*, L12.
[9] Y. Xia, T. Sakai, T. Fujieda, M. Wada, H. Yoshinaga, *J. Electrochem. Soc.* **2001**, *148*, 471.
[10] S. D. Beattie, J. R. Dahn, *J. Electrochem. Soc.* **2003**, *150*, A894.
[11] G. M. Ehrlich, C. Durand, X. Chen, T. A. Hugener, F. Spiess, S. L. Suib, *J. Electrochem. Soc.* **2000**, *147*, 886.
[12] H. Mukaido, T. Sumi, T. Yokoshima, T. Momma, T. Osaka, *Electrochem. Solid-State Lett.* **2003**, *6*, A218.
[13] Y.-L. Kim, H.-Y. Lee, S.-W. Jang, S.-J. Lee, H.-K. Baik, Y.-S. Yoon, Y.-S. Park, S.-M. Lee, *Solid State Ionics* **2003**, *160*, 235.
[14] O. Mao, R. L. Turner, I. A. Courtney, B. D. Fredericksen, M. I. Buckett, L. J. Krause, J. R. Dahn, *Electrochem. Solid-State Lett.* **1999**, *2*, 3.
[15] O. Mao, J. R. Dahn, *J. Electrochem. Soc.* **1999**, *146*, 414.
[16] M. Winter, J. O. Besenhard, *Electrochim. Acta* **1999**, *45*, 31.
[17] J. Yang, M. Winter, J. O. Besenhard, *Solid State Ionics* **1996**, *90*, 281.
[18] H.-C. Shin, J. Dong, M. Liu, *Adv. Mater.* **2003**, *15*, 1610.
[19] M. Pourbaix, in *Atlas of Electrochemical Equilibrium in Aqueous Solution*, Pergamon Press, Oxford, New York **1966**.
[20] Although there are no literatures available, as far as we know, to report the hydrogen over-voltage of the Cu-Sn alloy, the hydrogen over-voltage of the present Cu–Sn alloy seems to be low enough to liberate hydrogen gas on it under the electrodeposition conditions we adopted. This is supported by the fact that the vigorous gas evolution is observed by the naked eye not only on the copper substrate, but also the freshly formed Cu–Sn alloy on the duration of electrodeposition.
[21] A.-K. Larsson, L. Stenberg, S. Lidin, *Acta Crystallogr.* **1994**, *B50*, 636.
[22] M. M. Thackeray, J. T. Vaughey, A. J. Kahaian, K. D. Kepler, R. Benedek, *Electrochem. Commun.* **1999**, *1*, 111.
[23] D. Larcher, L. Y. Beaulieu, D. D. MacNeil, J. R. Dahn, *J. Electrochem. Soc.* **2000**, *147*, 1658.
[24] L. Fransson, E. Nordstrom, K. Edstrom, L. Haggstrom, J. T. Vaughey, M. M. Thackeray, *J. Electrochem. Soc.* **2002**, *149*, A736.
[25] A. H. Whitehead, J. M. Elliott, J. R. Owen, *J. Power Sources* **1999**, *81–82*, 33.
[26] A nominal specific capacity of 400 mA h g^{-1} was assumed to convert the current density into C rate, because this capacity value is the maximum reversible capacity ever reported at the moderate cycling conditions [8–10]. At the extremely low cycling rates of, e.g., C/100, however, about 600 mA h g^{-1} has been reported [23,24].

